✤ *Author's Choice*

methods

Unlabeled lysophosphatidic acid receptor binding in free solution as determined by a compensated interferometric reader

Manisha Ray,* Kazufumi Nagai,[1,*] Yasuyuki Kihara,* Amanda Kussrow,[†] Michael N. Kammer,[†] Aaron Frantz,[*,§] Darryl J. Bornhop,[†] and Jerold Chun[2,*]

Degenerative Disease Program,* Sanford Burnham Prebys Medical Discovery Institute, La Jolla, CA 92037; Department of Chemistry and Vanderbilt Institute for Chemical Biology,[†] Vanderbilt University, Nashville, TN 37235; and Biomedical Sciences Graduate Program,[§] University of California San Diego, La Jolla, CA 92037

ORCID ID: 0000-0003-3964-0921 (J.C.)

Abstract Native interactions between lysophospholipids (LPs) and their cognate LP receptors are difficult to measure because of lipophilicity and/or the adhesive properties of lipids, which contribute to high levels of nonspecific binding in cell membrane preparations. Here, we report development of a free-solution assay (FSA) where label-free LPs bind to their cognate G protein-coupled receptors (GPCRs), combined with a recently reported compensated interferometric reader (CIR) to quantify native binding interactions between receptors and ligands. As a test case, the binding parameters between lysophosphatidic acid (LPA) receptor 1 (LPA_1; one of six cognate LPA GPCRs) and LPA were determined. FSA-CIR detected specific binding through the simultaneous real-time comparison of bound versus unbound species by measuring the change in the solution dipole moment produced by binding-induced conformational and/or hydration changes. FSA-CIR identified K_D values for chemically distinct LPA species binding to human LPA_1 and required only a few nanograms of protein: 1-oleoyl (18:1; K_D = 2.08 ± 1.32 nM), 1-linoleoyl (18:2; K_D = 2.83 ± 1.64 nM), 1-arachidonoyl (20:4; K_D = 2.59 ± 0.481 nM), and 1-palmitoyl (16:0; K_D = 1.69 ± 0.1 nM) LPA. These K_D values compared favorably to those obtained using the previous generation back-scattering interferometry system, a chip-based technique with low-throughput and temperature sensitivity. In conclusion, FSA-CIR offers a new increased-throughput approach to assess quantitatively label-free lipid ligand-receptor binding, including nonactivating antagonist binding, under near-native conditions.—Ray, M., K. Nagai, Y. Kihara, A. Kussrow, M. N. Kammer, A. Frantz, D. J. Bornhop, and Jerold Chun. **Unlabeled lysophosphatidic acid receptor binding in free solution as determined by a compensated interferometric reader. *J. Lipid Res.* 2020.** 61: **1244–1251.**

Supplementary key words Keywords: receptor binding assay • G protein-coupled receptor • lysophospholipids • molecular interaction • interferometry • free-solution assay-compensated interferometric reader • lipid signaling

G protein-coupled receptors (GPCRs) represent a large super-family of membrane-bound signal transducing receptors that are activated by the binding of small molecules. Lysophospholipid (LP) receptors are a subset of GPCRs that mediate the actions of LP signaling lipids and have myriad biological roles throughout the body (1–3). LP receptors include five sphingosine-1-phosphate receptors that are already the target of three US Food and Drug Administration-approved medicines (fingolimod, siponimod, and ozanimod) (4–9) and six lysophosphatidic acid (LPA) receptors for which therapies are under clinical development (10). LPs were among the first bioactive signaling lipids identified (1, 2) and consist of a hydrophilic phosphate head group, a chiral -OH group, and a hydrophobic acyl chain of different lengths and degrees of saturation (11).

The six cognate LPA receptors ($LPA_{1–6}$) activate a range of heterotrimeric G proteins (11); all six receptors have been knocked out in mice revealing diverse biological effects (2, 12–16); and the crystal structures were determined for

This work was supported by U.S. Department of Defense Grant W81XWH-17-1-0455 (J.C.) and National Institutes of Health, National Institute of Neurological Disorders and Stroke Grants R01NS084398 (J.C.) and R01NS103940 (Y.K.). Additional support was provided by National Science Foundation Grant CHE1610964 (D.J.B.). The content is solely the responsibility of the authors and does not necessarily represent the official views of the National Institutes of Health. The authors declare that they have no conflicts of interest with the contents of this article.

Manuscript received 3 May 2020 and in revised form 1 June 2020.

Published, JLR Papers in Press, June 8, 2020
DOI https://doi.org/10.1194/jlr.D120000880

Abbreviations: BSI, back-scattering interferometry; CIR, compensated interferometric reader; DLS, dynamic light scattering; FSA, free-solution assay; GPCR; G protein-coupled receptor; LP, lysophospholipid; LPA, lysophosphatidic acid; $LPA_{1–6}$, lysophosphatidic acid receptors; RLB, radioligand binding.

[1]Present address of K. Nagai: Ono Pharmaceutical Company, Ltd., Osaka 618-8585, Japan.
[2]To whom correspondence should be addressed.
e-mail: jchun@SBPdiscovery.org

two LPA receptors (17–19). Despite these advances, it remains difficult to determine the native binding of unlabeled LPs to their cognate receptors in free solution. There are high levels of nonspecific signal produced by partitioning of labeled lipid ligands within cell membranes that enable normal GPCR function. Moreover, receptor binding studies usually employ highly overexpressed and/or modified receptors (e.g., tagged with EGFP), in addition to labeled ligands, which can affect results in unpredictable ways (20). Available biophysical techniques (21–23) like surface plasmon resonance (24, 25), fluorescence resonance energy transfer (26), fluorescence polarization (27), fluorescence cross-correlation spectroscopy (28), and radioligand binding (RLB) (29) all require immobilization and/or ligand labeling, which can affect K_D values as a result of chemical perturbations, such as those from fluorescent dye molecules or structural inflexibility produced by molecular tethers and immobilization.

Interferometric interaction assays have received significant interest over the past two decades to measure the affinity of molecular binding under more native conditions (i.e., in free solution and without labeling) (30–36). Free-solution assays (FSAs) allow for measurement of inherent solution-phase properties such as the conformational or hydration changes produced by binding (31–33). These changes can be detected by the newly developed compensated interferometric reader (CIR) (36, 37). The combination of FSA-CIR should allow for the determination of binding parameters including the dissociation constant (K_D) between various lipid chemical forms and their known and unknown cognate receptors under label-free conditions.

We recently reported LPA-specific binding to LPA_1 using a predecessor technology, back-scattering interferometry (BSI), which had low throughput (six samples with five replicates; ~3 h) and variability produced by temperature (35). To overcome these challenges, a new CIR (36) was developed by the Bornhop laboratory at Vanderbilt University (36), which enabled simultaneous measurement of sample and reference-pairs using the same probe beam, thus nullifying sensitivity to temperature fluctuations. The use of a capillary cell for smooth uninterrupted sample introduction and detection enhanced the signal-to-noise ratio and increased throughput compared with the BSI platform.

Here, we report a novel free-solution label-free assay using CIR that produces a 12-fold higher throughput (12 samples with 5 replicates; ~30 min). FSA-CIR was used to determine LPA-LPA_1 K_Ds for multiple LPA forms with differing acyl chain length and saturation, representing a proof-of-concept for the broader use of FSA-CIR to interrogate LP and other lipid ligand-receptor molecular interactions including orthosteric, allosteric, and antagonist binding.

MATERIALS AND METHODS

LPA handling and stock preparation

Various chemical forms of LPA were assayed: 1-oleoyl-LPA (18:1), 1-palmitoyl-LPA (16:1), 1-arachidonoyl-LPA (20:4), 1-linoleoyl-LPA (18:2), and 1-oleoyl-lysophosphatidylcholine (18:1 LPC) (Avanti Polar Lipids Inc.). Saturated or mono-unsaturated samples (16:0, 18:1 LPAs, and 18:1 LPC) were completely dissolved in ethanol:water (1:1 v/v) by sonicating for 3–5 min, aliquoted in glass vials layered with N_2, and stored under N_2 atmosphere at −20°C for several uses (up to 9 months). Unstable and unsaturated LPA samples (18:2 and 20:4; received in $CHCl_3$) were desiccated and then reconstituted in fresh ethanol:water (1:1 v/v) for immediate use in binding assays. Redissolving desiccated LPAs in aqueous BSA solutions for storage purposes was eliminated because it resulted in 95–97% loss of LPA during reconstitution (38). Stored or reconstituted LPAs in ethanol:water solution show a monodispersed distribution of LPA as measured by dynamic light scattering (DLS). Saturated LPAs are relatively stable under atmosphere, whereas unsaturated ones are highly unstable, extremely hygroscopic, and, therefore, cannot be stored for subsequent use in this assay.

Preparation of cell lines

Stable B103 cell lines expressing LPA_1 were developed, cultured, and used for receptor-containing nanovesicle preparation, as previously described (35). Briefly, a polyclonal B103 rat neuroblastoma stable cell line expressing human LPA_1 with an HA epitope tagged N terminus (HA-LPA_1-B103) was established by antibiotic selection and cell sorting (35). Microsomal fractions were prepared from HA-LPA_1-B103 cells and controls (vector transfected cells; Vec-B103) by starving the cells for 16 h in DMEM high glucose containing 0.5% BSA (Gemini Bio Products); the cells were washed with ice-cold PBS, collected by scraping, and stored at −80°C for vesicle preparation.

Nanovesicle preparation from HA-LPA_1-B103 and Vec-B103 cells

HA-LPA_1-B103 or Vec-B103 cells were probe-sonicated to generate nanovesicles (39) for analysis (**Fig. 1A**). Briefly, HA-LPA_1-B103 or Vec-B103 cell pellets (~$6–7 \times 10^6$ cells) were resuspended in 1 ml of ice-cold PBS containing cOmplete™ protease inhibitor mixture (Roche) and transferred to a glass dram vial. Cell suspensions in an ice bath were then probe sonicated (Qsonica Q125 sonicator, 30–40% amplitude with an intense pulse sound; pulse: 5 s on, 1 s off, for 90 s) and the resulting solutions were centrifuged at 4°C for 1 h at 10,000 *g*. The supernatant containing nanovesicles with HA-LPA_1 or vector was collected and stored at 4°C until use later that day. The expression of HA-LPA_1 was confirmed by Western blot (35) with Vec-B103 cells serving as a negative control. Vesicles were characterized using DLS (Dynapro Nanostar, Wyatt Technologies) and total protein concentration was measured by Bradford assay using fatty acid-free BSA as a standard.

FSA preparation

The FSA preparation was modified from a tissue-based assay protocol (33). Nanovesicle solutions and their buffer-matched vesicle devoid solutions were prepared independently and combined with the LPA dilution series to create index-matched sample-reference pairs (**Fig. 2**).

LPA ligand solution preparation. In blood or plasma, 30–40% of LPA circulates bound to the carrier protein albumin (Fig. 2A). Therefore, freshly prepared fatty acid-free BSA was used in the final binding assay preparation for in vivo compatibility. LPAs have poor solubility, low critical micelle concentration (~300 μM) and bind to Eppendorf tube walls when prepared in aqueous buffers (40), resulting in concentration variations of the analyte and error in the measurement. LPA bound to fatty acid-free BSA in solution can result in aggregation (diameter ranges from 10 to 10,000 nm) when stored at −20°C, even after reducing the particle size

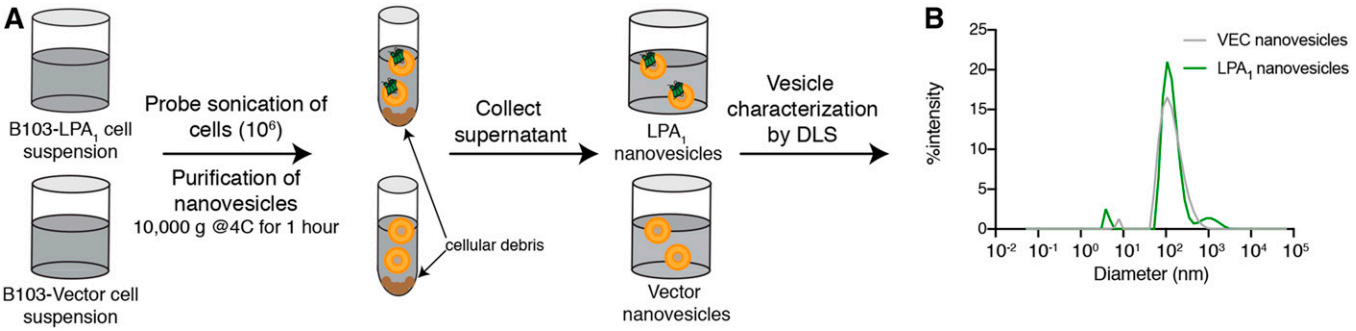

Fig. 1. Sample workflow used to prepare and characterize LPA_1-containing and vector nanovesicles. A rat neural cell line, B103, was used to produce LPA_1-containing vesicles by heterologous expression of a human LPA_1 cDNA that was stably expressed. Vector transfected B103 cells were used as a control. A: B103-LPA_1 and B103-vector transfected cell suspensions were probe sonicated (Qsonica Q125 sonicator; ~30–40% amplitude; pulse: 5 s on, 1 s off for 90 s), and the resulting nanovesicles were isolated by centrifugation. The nanovesicle- containing supernatant was characterized using the Bradford assay for protein concentration. B: DLS was used to determine vesicle size distributions. Vesicles of diameters ~100–150 nm were utilized.

by sonication. Therefore, LPAs were assessed in freshly prepared fatty acid-free BSA solution. A stock solution of LPA in ethanol:water (5 mM) was redissolved in 0.1% fresh fatty acid-free BSA (w/v) solution to prepare 200 nM of intermediate stock containing 0.01% fatty acid-free BSA in 0.002% ethanol/PBS (v/v). The 0.002% ethanol in 0.01% BSA/PBS solution was kept constant across all ligand dilutions to ensure that free solution measurements were index matched.

LPA_1 or vector- and buffer-matched reference solution preparation. LPA_1-containing or vector control nanovesicles in solution were made using cOmplete™ protease inhibitor solution in PBS, diluted with 1× PBS (pH 7.4) to a working concentration of 50 μg/ml (Fig. 2B). Buffer-matched no-vesicle solutions were prepared as reference solutions.

Binding assay preparation

A serial dilution series (100, 20, 4, 0.8, 0.16, 0.032, 0.0064, and 0 nM) of lipid ligands was prepared from a 200 nM of LPA solution by diluting with 0.002% ethanol/0.01% BSA/PBS (Fig. 2A). A "zero" concentration consisted of 0.002% ethanol/0.01% BSA/PBS. Each concentration of the diluted ligand was combined with an equal volume of the 50 μg/ml LPA_1-containing or vector control nanovesicle solutions (Fig. 2B) to produce binding and nonbinding test samples with buffer-matched no-vesicle reference solutions (Fig. 2C) with a final buffer composition of 0.001% ethanol/water/0.005% BSA in PBS. The final protein concentration was 25 μg/ml and the final ligand concentration ranged from 0 to 50 nM. The mixtures were allowed to reach equilibrium for 1 h at room temperature prior to analysis by CIR.

The CIR

The simple and cost-effective experimental arrangement of the CIR has been described elsewhere (41, 42) and consists of the compensated interferometer, a droplet generator (Mitox Dropix; Dolomite Microfluidics), and a syringe pump (Harvard Apparatus) (**Fig. 3**). This next generation BSI is a droplet-based technology that allows for simultaneous interrogation of sample and reference in continuous droplet trains separated by thermally and chemically stable oil (Fluorinert FC-40, Sigma-Aldrich).

The interferometer consists of a diode laser, a beam directing optic (one 1/2 mirror), a microfluidic channel (a glass capillary), and a CCD camera (Fig. 3). The auto sample introducer was programed with built-in software to introduce droplet trains of sample-reference pairs into a glass capillary. As demonstrated recently (37), droplet trains of sample-reference pairs were produced by a Dropix sample hook that guides the capillary tubing up and down between sample-reference pairs contained in a bottomless reservoir made of polyether ether ketone materials mounted on a second fluid reservoir (#3200354, Dolomite Microfluidics) containing the Fluorinert™ FC-40 oil (Sigma-Aldrich). The syringe pump pulls fluid from both reservoirs to maintain a constant flow of the droplet train through the capillary while maintaining a constant pressure without perturbation by any other sources. Simultaneous sample-reference interrogation (from region 1 and 2; Fig. 3A, B) was measured by direct probing with an expanded beam profile emanating from the laser diode. The assays were measured sequentially, starting with the reference sample. Briefly, the capillary was filled with rinse buffer (0.005% BSA in 0.001% ethanol/PBS) and the syringe pump flow rate was set to 20 μl/min for 8–10 min to achieve a stable flow. The assay was run by introducing 1 μl of sample-reference pairs (five replicates) followed by two rinses of 2 μl, each separated by a 40 nL droplet of oil. This process was repeated for all concentrations. Prior to analysis of other LPA forms, the glass capillary was completely cleaned with 1 ml of a 1:1 (v/v) mixture of $CHCl_3$:methanol and dried manually with a syringe vacuum to eliminate lipid carryover.

The resulting backscattered interference fringes were detected by the CCD array using a detection window of 200 pixels long (1,100 μm) along a glass capillary with an inner diameter of 250 μm, yielding an optical probe volume of 54 nL. The positional shift of the fringes (equivalent to molecular binding) was quantified using a fast Fourier-transform algorithm in a customized Labview™ program.

Statistical analyses

Each receptor-ligand interaction (isotherm) was repeated at least three times on different days with freshly prepared FSA and each had five to seven replicates. The total versus nonspecific binding CIR signal, as plotted on the y-axis, and different ligand concentrations on the x-axis were fitted using GraphPad Prism™.

$$\text{Total} = \text{specific} + \text{nonspecific}$$

$$\text{Nonspecific} = \text{NS} \times \text{X} + \text{Background}$$

$$\text{Specific} = \text{Bmax} \times \text{X} / (\text{X} + K_D)$$

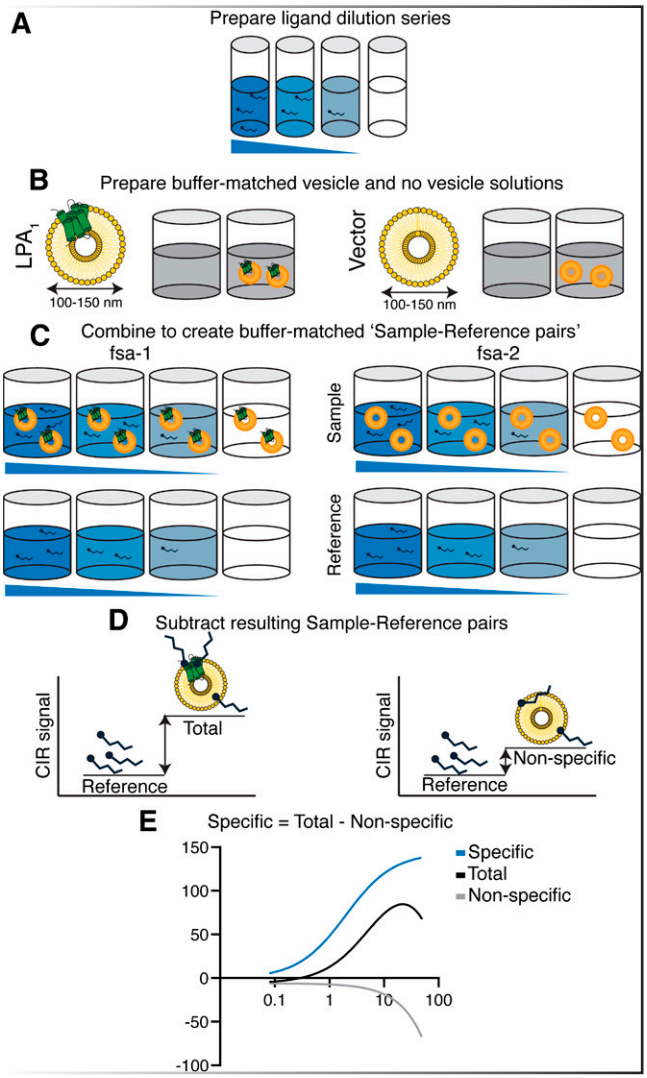

Fig. 2. Cell membrane vesicle-based FSA protocol. A: An LPA dilution series was prepared in 0.01% fatty acid-free BSA/0.002% ethanol (six to seven dilutions were prepared for the binding assay). B: Buffer-matched sample-reference pairs were prepared with LPA_1/no vesicle and vector/no vesicle solutions. C: LPA dilution series were mixed with LPA_1-containing and vector nanovesicles (test samples) and with the paired buffer-matched no vesicles solution (reference samples) in *fsa-1* and *fsa-2* and were equilibrated for 1 h. D: Sample-reference pairs were processed in the CIR (Fig. 3) with increasing concentrations of LPA and a fixed concentration of total protein (LPA_1/vector; 25 μg/ml). One binding curve was generated for each sample-reference pair: the vector-sample measures nonspecific signal and the LPA_1 sample measures total binding signal. E: The specific binding signal (blue) was calculated by subtracting the nonspecific binding signal from the total binding signal. K_D for LPA to LPA_1 was calculated by plotting the specific binding signal against LPA concentrations.

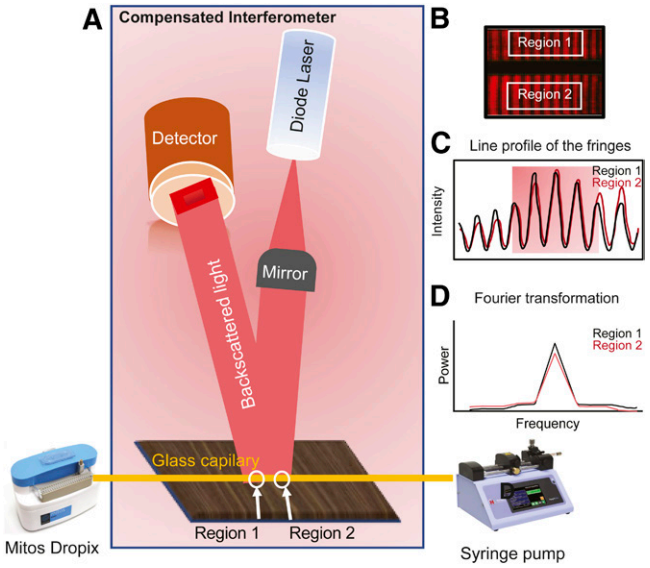

Fig. 3. CIR. A: CIR consists of a diode laser, a microfluidic channel (a glass capillary), a fringe detector, an automated droplet generator for sample introduction (Mitos Dropix), and a syringe pump. The Mitos Dropix introduces sample droplet trains into the glass capillary while the syringe pump maintains a constant sample flow through the capillary. Sample and reference pairs flow through regions 1 and 2 where they are simultaneously interrogated by the diode laser. Resultant images of the fringe patterns and their phase shifts under binding/nonbinding conditions (B) are converted to a line profile (C) where selected fringes are fast Fourier transformed for analyses (D).

RESULTS

Measurement of monodisperse nanovesicle size distributions

LPA_1 and control nanovesicles were prepared by probe sonication of microsomal fractions from HA-LPA_1-B103 and vector-B103 cells (Fig. 1A) to produce nanovesicles with a size distribution of 100–150 nm (as measured by DLS) (Fig. 1B). Monodisperse solutions of LPA_1 and vector nanovesicles with intense single and overlapping DLS peaks were essential to avoid rapid vesicle fusion and aggregation, as well as possible index mismatch of control solutions. Nanovesicles were used fresh to provide predictable and consistent results: 4°C storage resulted in aggregation and −80°C storage resulted in both aggregation and ice crystal formation.

FSA

Two sample-reference-pair solutions were used to determine specific binding: *fsa-1* (total binding) and *fsa-2* (nonspecific binding) (Fig. 2). The *fsa-1* sample-reference pair consisted of LPA_1-vesicle (test sample) and buffer-matched (reference sample) solutions with increasing concentrations of LPA ligand (Fig. 2C). The *fsa-2* sample-reference pair was identical, except that it contained vector control nanovesicles rather than LPA_1 nanovesicles. The total protein concentration of LPA_1 or vector-nanovesicles was fixed at 25 μg/ml. The difference in interferometric signal between the sample-reference pair in *fsa-1* provided a quantitative measure of the total binding of LPA ligands to LPA_1, whereas *fsa-2* provided nonspecific binding of LPA ligands to vector nanovesicles (Fig. 2D, E). Precise preparation of buffer-matched sample-reference pairs and the subsequent subtraction eliminated background signal created by the complex matrix of LPA_1. Thus, when measured in the CIR, *fsa-1* versus *fsa-2* allowed determination of specific LPA-LPA_1 K_D values (**Table 1**).

TABLE 1. Binding constants (K_D) for different LPA species

Membrane Bound Receptor	Ligands LPA/LPC	K_D ± SEM	Previously Reported K_D Values	Previously Reported EC_{50} Values
LPA_1	18:1 LPA	2.08 ± 1.32 nM	K_D = 0.87 ± 0.37 nM (from BSI) K_D = 68.9 nM (from RLB)	200 nM
	18:2 LPA	2.83 nM ± 1.64	None reported	200 nM
	20:4 LPA	2.59 nM ± 0.481	None reported	200 nM
	16:0 LPA	1.69 nM ± 0.1	None reported	400 nM
	18:1 LPC	∼0 nM	None reported	None reported

Binding constants were determined from specific binding data from the plots (Fig. 4) compared with reported BSI (35), RLB (29), and EC_{50} (46) assessments.

LPA-specific binding to LPA_1 in cell membrane nanovesicles identified by FSA-CIR

Five LPA ligands that differed in acyl chain length and saturation were assayed to quantify their binding affinity to a cognate receptor, LPA_1, as compared with a control LP, LPC (**Fig. 4**). In the CIR, an expanded diode laser beam produces "elongated" fringes resulting from illumination of the droplet train filled capillary. Elongated fringe patterns differ between sample and reference pairs, which translated into RI differences that also changed in proportion to the ligand concentration. Fringe-shift measurements from ligands interacting with LPA_1 produced the total binding signal (*fsa-1*; Fig. 4A–E, black lines) that showed successively positive RI changes that increased with lipid concentration; subtraction of minor nonspecific RI changes (*fsa-2*; Fig. 4A–E, gray lines) enabled calculation of specific signals (Fig. 4A–E; colored lines) and K_D values were calculated (Table 1; Fig. 4F).

All LPA forms exhibited K_D values in the low nanomolar range [1-oleoyl (18:1) (K_D = 2.08 nM ± 1.32)], 1-linoleoyl (18:2) (K_D = 2.83 nM ± 1.64), 1-arachidonoyl (20:4) (K_D = 2.59 nM ± 0.481), and 1-palmitoyl (16:0) (K_D = 1.69 nM ± 0.1); Table 1] regardless of the acyl chain length or saturation. This is consistent with the documented selectivity of the LPA_1 binding pocket for the phosphate headgroup rather than the acyl chain (17). No specific signals were observed for total versus nonspecific binding of 18:1 LPC. The specific low nanomolar (2–3 nM) K_D values of LPA_1-LPA binding demonstrate both the sensitivity and specificity of FSA-CIR, thus supporting its utility in detecting lipid receptor-ligand binding under label-free conditions.

DISCUSSION

Molecular interaction studies with lipids represent a challenge because of the physical-chemical nature of lipids including ligand solubility, membrane intercalation, loss to surfaces, and stability. Classical receptor-lipid binding assays using radiolabeled ligands are difficult because of the high levels of nonspecific binding within membranes, ligand degradation, and the requirement for receptors to be properly folded within a cell membrane lipid bilayer. Here, we report FSA-CIR that measures such interactions using label-free signaling LPAs and a cognate GPCR (using LPA_1) in nanovesicles, freely floating in solution. Individual measurement of total and nonspecific binding reduces the background signal produced by assay conditions where GPCRs are present in a complex milieu of other lipids, proteins, and biological fluids. Nanovesicle-based receptor binding FSAs in combination with CIR should be generalizable to measure many other signaling lipids that interact with cell-surface receptors known to regulate myriad cellular and physiological processes (2, 6, 10, 11).

FSA-CIR studies identified a requirement for several key variables: uniform size of nanovesicle, buffer-matched control solutions, fresh nanovesicle preparations, and precise lipid handling. Control of these variables enabled FSA-CIR to achieve substantial improvements over other methods including the previous generation of BSI. Techniques that utilize target and/or ligand immobilization [surface plasmon resonance, BLI (43, 44)] and/or labeling [fluorescence resonance energy transfer, fluorescence polarization, RLB (45)] can alter the binding characteristics of the ligands, receptors, or both, which can obfuscate native binding characteristics. Thus, FSA-CIR better approximates a native binding environment. By comparison, the previous generation BSI assay had limitations related to difficulty of use, sample preparation and delivery, throughput, and temperature sensitivity. FSA-CIR employs semi-automated sample delivery and simultaneous interrogation of sample and reference (29) to reduce instrument noise produced by operator skill level, laser instability, and temperature fluctuations.

FSA-CIR provided comparable detection of K_D values with its predecessor BSI (Table 1) (35). FSA-CIR-measured K_D values ranged from 0.87 to 2.59 nM for all forms of LPA. These K_D values show a 35- to 40-fold higher affinity than previous assessments by RLB (29) that reported K_D values of 68.9 nM for 18:1 LPA-LPA_1 binding and similar values for other LPA receptors (LPA_2 K_D = 63.7 nM, LPA_4 K_D = 99.6 nM, and LPA_5 K_D = 88.6 nM). The higher nanomolar K_D values (weaker affinity) detected by RLB likely reflect technical and procedural artifacts such as the rapid off-rate caused by several washing steps that may result in high nonspecific binding. This comparison demonstrates the utility of our FSA-CIR approach as a highly sensitive and reliable binding assay. To our knowledge, these data are the first determination of K_D values for other native forms of LPA (16:0,18:2, and 20:4). Our results indicate no specificity of LPA_1 toward saturated or unsaturated LPA forms, which is comparable to previously reported EC_{50} values from a Ca^{+2} response assay that showed similar potency for all LPA

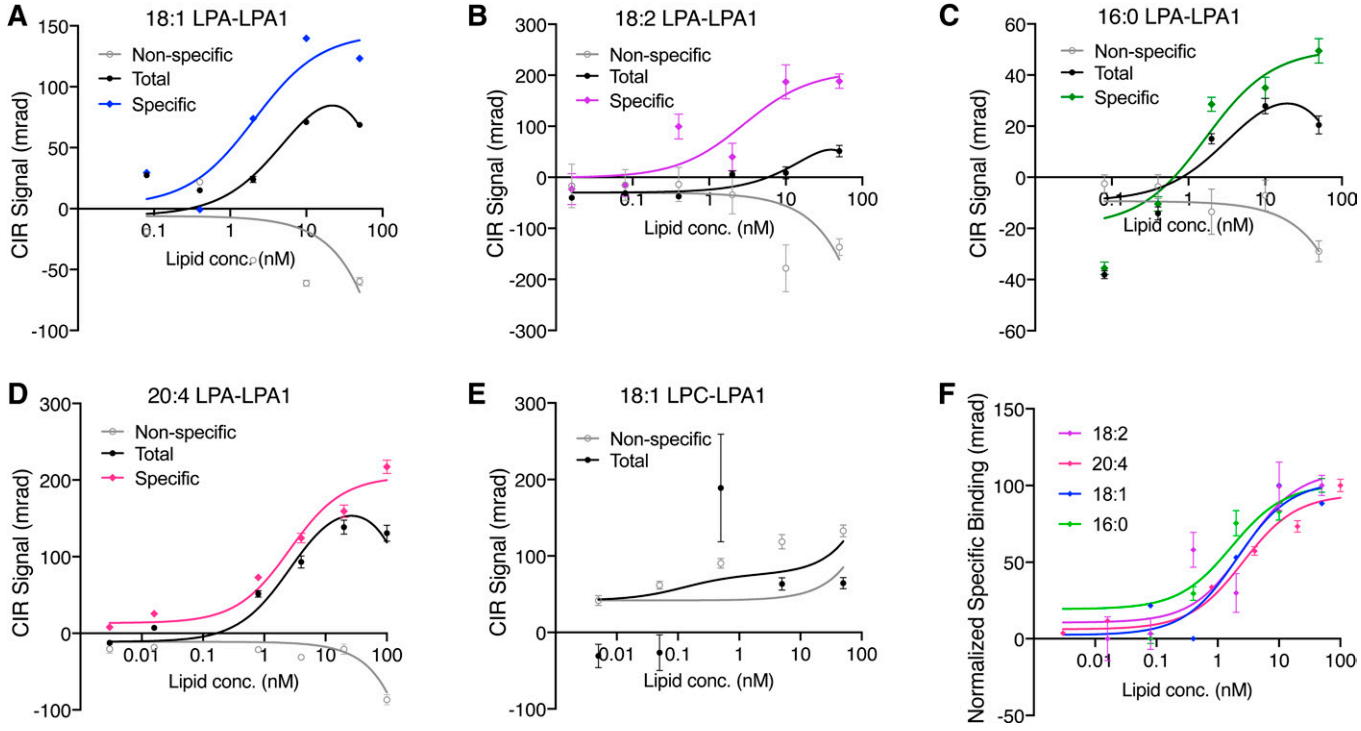

Fig. 4. CIR determination of specific binding of LPA ligands 18:1, 18:2, 16:0, and 20:4 to LPA_1 compared with LPC. CIR signals versus ligand concentration were plotted. A–E: Representative plots of changes in RI (milliradians) produced by binding as revealed by CIR for 18:1 (A), 18:2 (B), 16:0 (C), 20:4 (D) LPA, and 18:1 LPC (E) (negative control). Nonspecific (gray), total (black), and calculated specific (colored) binding are shown. F: Normalized specific binding signal for all LPA ligands overlapped (see Table 1 for K_D values). Each graph shows an average of three independent binding isotherms (experimental replicates), each with five to seven measurements (technical replicates).

forms to active LPA_1 and LPA_2 (Table 1) (46). Other reports identified ligand specificity for other LPA receptors (18, 29, 46–49) and these distinct LPA ligand-receptor interactions remain to be assessed in future FSA-CIR studies.

Importantly, FSA-CIR was able to achieve this sensitivity and specificity with only nanograms (picomoles) of receptor protein. If we assume 100% binding and no free LPA molecules at the 100 nM LPA concentration, only 1.35 ng of total protein (containing ~3.2×10^9 LPA_1 molecules) are needed to achieve a saturated binding signal. Similarly, at the minimum quantifiable binding signal (500 pM of LPA), 1.6×10^7 (27 attomoles) LPA-LPA_1 complexes are present. Combined, our assay required 21 μg of total protein to assess all replicates and LPA concentrations, illustrating the small amounts of lipid ligand-receptor complex required to observe a binding signal, and the versatility of this FSA-CIR system.

Altogether, FSA-CIR provided comparable detection to BSI while allowing for ~12-fold increased throughput. Previously difficult to measure lipid ligand-receptor interactions (50) can now be approached with comparative ease under more native conditions that do not require radioactivity or labeling of ligands or receptors. Notably, the in vivo presence of bivalent cations (e.g., Ca^{2+} and Mg^{2+}) will alter the availability and physiology of LPA ligands and, therefore, will likely impact receptor binding affinities (51). Assessment of LPA-LPA_1 binding under improved physiological conditions is imperative for future drug discovery efforts. These features raise the possibility of examining future samples from primary cells and even tissues naturally or engineered to be devoid of a single target receptor, as well as allowing interrogation of binding interactions that occur in complex matrices like human fluids and tissues. FSA-CIR should thus be useful in identifying and validating a range of lipid ligand-receptor interactions, including those with clinical potential.

The authors thank Dr. Andrew Richards and Ms. Mahsa Nafisi for help with sample tray manufacturing (University of California San Diego). Additional thanks to Mr. Joshua Kurtz for sample tray cleaning and Dr. Gwendolyn Kaeser for figure preparation and editorial, Dr. Laura Wolszon, and Ms. Danielle Jones for editorial assistance.

Data availability

All data are contained within the article.

REFERENCES

1. Chun, J., T. Hla, W. Moolenaar, and S. Spiegel, editors. 2014. Lysophospholipid Receptors: Signaling and Biochemistry. Wiley, Hoboken, NJ.
2. Yung, Y. C., N. C. Stoddard, H. Mirendil, and J. Chun. 2015. Lysophosphatidic acid signaling in the nervous system. *Neuron.* **85:** 669–682.
3. Sheng, X., Y. C. Yung, A. Chen, and J. Chun. 2015. Lysophosphatidic acid signalling in development. *Development.* **142:** 1390–1395.

4. Choi, J. W., S. E. Gardell, D. R. Herr, R. Rivera, C. W. Lee, K. Noguchi, S. T. Teo, Y. C. Yung, M. Lu, G. Kennedy, et al. 2011. FTY720 (fingolimod) efficacy in an animal model of multiple sclerosis requires astrocyte sphingosine 1-phosphate receptor 1 (S1P1) modulation. *Proc. Natl. Acad. Sci. USA.* **108:** 751–756.
5. Chun, J., and V. Brinkmann. 2011. A mechanistically novel, first oral therapy for multiple sclerosis: the development of fingolimod (FTY720, Gilenya). *Discov. Med.* **12:** 213–228.
6. Cohen, J. A., and J. Chun. 2011. Mechanisms of fingolimod's efficacy and adverse effects in multiple sclerosis. *Ann. Neurol.* **69:** 759–777.
7. Chun, J., Y. Kihara, D. Jonnalagadda, and V. A. Blaho. 2019. Fingolimod: lessons learned and new opportunities for treating multiple sclerosis and other disorders. *Annu. Rev. Pharmacol. Toxicol.* **59:** 149–170.
8. Groves, A., Y. Kihara, and J. Chun. 2013. Fingolimod: direct CNS effects of sphingosine 1-phosphate (S1P) receptor modulation and implications in multiple sclerosis therapy. *J. Neurol. Sci.* **328:** 9–18.
9. Bristol Myers Squibb™. 2020. U.S. Food and Drug Administration Approves Bristol Myers Squibb's ZEPOSIA® (ozanimod), a New Oral Treatment for Relapsing Forms of Multiple Sclerosis. Press release; March 26, 2020.
10. Kihara, Y., H. Mizuno, and J. Chun. 2015. Lysophospholipid receptors in drug discovery. *Exp. Cell Res.* **333:** 171–177.
11. Kihara, Y., M. Maceyka, S. Spiegel, and J. Chun. 2014. Lysophospholipid receptor nomenclature review: IUPHAR review 8. *Br. J. Pharmacol.* **171:** 3575–3594.
12. Yung, Y. C., N. C. Stoddard, and J. Chun. 2014. LPA receptor signaling: pharmacology, physiology, and pathophysiology. *J. Lipid Res.* **55:** 1192–1214.
13. Stoddard, N. C., and J. Chun. 2015. Promising pharmacological directions in the world of lysophosphatidic Acid signaling. *Biomol. Ther. (Seoul).* **23:** 1–11.
14. Noguchi, K., and J. Chun. 2011. Roles for lysophospholipid S1P receptors in multiple sclerosis. *Crit. Rev. Biochem. Mol. Biol.* **46:** 2–10.
15. Mutoh, T., R. Rivera, and J. Chun. 2012. Insights into the pharmacological relevance of lysophospholipid receptors. *Br. J. Pharmacol.* **165:** 829–844.
16. Yang, A. H., I. Ishii, and J. Chun. 2002. In vivo roles of lysophospholipid receptors revealed by gene targeting studies in mice. *Biochim. Biophys. Acta.* **1582:** 197–203.
17. Chrencik, J. E., C. B. Roth, M. Terakado, H. Kurata, R. Omi, Y. Kihara, D. Warshaviak, S. Nakade, G. Asmar-Rovira, M. Mileni, et al. 2015. Crystal structure of antagonist bound human lysophosphatidic acid receptor 1. *Cell.* **161:** 1633–1643.
18. Taniguchi, R., A. Inoue, M. Sayama, A. Uwamizu, K. Yamashita, K. Hirata, M. Yoshida, Y. Tanaka, H. E. Kato, Y. Nakada, et al. 2017. Structural insights into ligand recognition by the lysophosphatidic acid receptor LPA6. *Nature.* **548:** 356–360.
19. Blaho, V. A., and J. Chun. 2018. 'Crystal' clear? Lysophospholipid receptor structure insights and controversies. *Trends Pharmacol. Sci.* **39:** 953–966.
20. Wise, A., K. Gearing, and S. Rees. 2002. Target validation of G-protein coupled receptors. *Drug Discov. Today.* **7:** 235–246.
21. de Jong, L. A. A., D. R. A. Uges, J. P. Franke, and R. Bischoff. 2005. Receptor-ligand binding assays: technologies and applications. *J. Chromatogr. B Analyt. Technol. Biomed. Life Sci.* **829:** 1–25.
22. Cho, H., M. Wu, B. Bilgin, S. P. Walton, and C. Chan. 2012. Latest developments in experimental and computational approaches to characterize protein-lipid interactions. *Proteomics.* **12:** 3273–3285.
23. Saliba, A. E., I. Vonkova, and A. C. Gavin. 2015. The systematic analysis of protein-lipid interactions comes of age. *Nat. Rev. Mol. Cell Biol.* **16:** 753–761.
24. Kuroki, K., and K. Maenaka. 2011. Analysis of receptor-ligand interactions by surface plasmon resonance. *Methods Mol. Biol.* **748:** 83–106.
25. Patching, S. G. 2014. Surface plasmon resonance spectroscopy for characterisation of membrane protein-ligand interactions and its potential for drug discovery. *Biochim. Biophys. Acta.* **1838 (1 Pt. A):** 43–55.
26. Kauk, M., and C. Hoffmann. 2018. Intramolecular and Intermolecular FRET Sensors for GPCRs - monitoring conformational changes and beyond. *Trends Pharmacol. Sci.* **39:** 123–135.
27. Stoddart, L. A., C. W. White, K. Nguyen, S. J. Hill, and K. D. Pfleger. 2016. Fluorescence- and bioluminescence-based approaches to study GPCR ligand binding. *Br. J. Pharmacol.* **173:** 3028–3037.
28. Ciruela, F., K. A. Jacobson, and V. Fernandez-Duenas. 2014. Portraying G protein-coupled receptors with fluorescent ligands. *ACS Chem. Biol.* **9:** 1918–1928.
29. Yanagida, K., K. Masago, H. Nakanishi, Y. Kihara, F. Hamano, Y. Tajima, R. Taguchi, T. Shimizu, and S. Satoshi. 2009. Identification and characterization of a novel lysophosphatidic acid receptor, p2y5/LPA6. *J. Biol. Chem.* **284:** 17731–17741.
30. Kammer, M. N., I. R. Olmsted, A. K. Kussrow, M. J. Morris, G. W. Jackson, and D. J. Bornhop. 2014. Characterizing aptamer small molecule interactions with backscattering interferometry. *Analyst.* **139:** 5879–5884.
31. Olmsted, I. R., M. Hassanein, A. Kussrow, M. Hoeksema, M. Li, P. P. Massion, and D. J. Bornhop. 2014. Toward rapid, high-sensitivity, volume-constrained biomarker quantification and validation using backscattering interferometry. *Anal. Chem.* **86:** 7566–7574.
32. Sulmann, S., A. Kussrow, D. J. Bornhop, and K. W. Koch. 2017. Label-free quantification of calcium-sensor targeting to photoreceptor guanylate cyclase and rhodopsin kinase by backscattering interferometry. *Sci. Rep.* **7:** 45515.
33. Wang, M., A. K. Kussrow, M. F. Ocana, J. R. Chabot, C. S. Lepsy, D. J. Bornhop, and D. M. O'Hara. 2017. Physiologically relevant binding affinity quantification of monoclonal antibody PF-00547659 to mucosal addressin cell adhesion molecule for in vitro in vivo correlation. *Br. J. Pharmacol.* **174:** 70–81.
34. Ellery, J., L. Dickson, T. Cheung, L. Ciuclan, P. Bunyard, S. Mack, W. J. Buffham, W. Farnaby, P. Mitchell, D. Brown, et al. 2018. Identification of compounds acting as negative allosteric modulators of the LPA1 receptor. *Eur. J. Pharmacol.* **833:** 8–15.
35. Mizuno, H., Y. Kihara, A. Kussrow, A. Chen, M. Ray, R. Rivera, D. J. Bornhop, and J. Chun. 2019. Lysophospholipid G protein-coupled receptor binding parameters as determined by backscattering interferometry. *J. Lipid Res.* **60:** 212–217.
36. Kammer, M. N., A. Kussrow, I. Gandhi, R. Drabek, R. H. Batchelor, G. W. Jackson, and D. J. Bornhop. 2019. Quantification of opioids in urine using an aptamer-based free-solution assay. *Anal. Chem.* **91:** 10582–10588.
37. Kammer, M. N., A. K. Kussrow, R. L. Webster, H. Chen, M. Hoeksema, R. Christenson, P. P. Massion, and D. J. Bornhop. 2019. Compensated interferometry measures of CYFRA 21-1 improve diagnosis of lung cancer. *ACS Comb. Sci.* **21:** 465–472.
38. Lummis, N. C., P. Sánchez-Pavón, G. Kennedy, A. J. Frantz, Y. Kihara, V. A. Blaho, and J. Chun. 2019. LPA1/3 overactivation induces neonatal posthemorrhagic hydrocephalus through ependymal loss and ciliary dysfunction. *Sci. Adv.* **5:** eaax2011.
39. Baksh, M. M., A. K. Kussrow, M. Mileni, M. G. Finn, and D. J. Bornhop. 2011. Label-free quantification of membrane-ligand interactions using backscattering interferometry. *Nat. Biotechnol.* **29:** 357–360.
40. Li, Z., E. Mintzer, and R. Bittman. 2004. The critical micelle concentrations of lysophosphatidic acid and sphingosylphosphorylcholine. *Chem. Phys. Lipids.* **130:** 197–201.
41. Kammer, M. N., A. K. Kussrow, and D. J. Bornhop. 2018. Longitudinal pixel averaging for improved compensation in backscattering interferometry. *Opt. Lett.* **43:** 482–485.
42. Kammer, M. N., A. K. Kussrow, I. R. Olmsted, and D. J. Bornhop. 2018. A highly compensated interferometer for biochemical analysis. *ACS Sens.* **3:** 1546–1552.
43. Locatelli-Hoops, S., A. A. Yeliseev, K. Gawrisch, and I. Gorshkova. 2013. Surface plasmon resonance applied to G protein-coupled receptors. *Biomed. Spectrosc. Imaging.* **2:** 155–181.
44. Navratilova, I., J. Besnard, and A. L. Hopkins. 2011. Screening for GPCR ligands using surface plasmon resonance. *ACS Med. Chem. Lett.* **2:** 549–554.
45. Swift, J. L., M. C. Burger, D. Massotte, T. E. Dahms, and D. T. Cramb. 2007. Two-photon excitation fluorescence cross-correlation assay for ligand–receptor binding: cell membrane nanopatches containing the human micro-opioid receptor. *Anal. Chem.* **79:** 6783–6791.
46. Bandoh, K., J. Aoki, A. Taira, M. Tsujimoto, H. Arai, and K. Inoue. 2000. Lysophosphatidic acid (LPA) receptors of the EDG family are differentially activated by LPA species. Structure-activity relationship of cloned LPA receptors. *FEBS Lett.* **478:** 159–165.
47. Noguchi, K., S. Ishii, and T. Shimizu. 2003. Identification of p2y9/GPR23 as a novel G protein-coupled receptor for lysophosphatidic

acid, structurally distant from the Edg family. *J. Biol. Chem.* **278:** 25600–25606.
48. Choi, J. W., D. R. Herr, K. Noguchi, Y. C. Yung, C. W. Lee, T. Mutoh, M-E. Lin, S. T. Teo, K. E. Park, A. N. Mosley, et al. 2010. LPA receptors: subtypes and biological actions. *Annu. Rev. Pharmacol. Toxicol.* **50:** 157–186.
49. Bandoh, K., J. Aoki, H. Hosono, S. Kobayashi, T. Kobayashi, K. Murakami-Murofushi, M. Tsujimoto, H. Arai, and K. Inoue. 1999. Molecular cloning and characterization of a novel human G-protein-coupled receptor, EDG7, for lysophosphatidic acid. *J. Biol. Chem.* **274:** 27776–27785.
50. Hecht, J. H., J. A. Weiner, S. R. Post, and J. Chun. 1996. Ventricular zone gene-1 (vzg-1) encodes a lysophosphatidic acid receptor expressed in neurogenic regions of the developing cerebral cortex. *J. Cell Biol.* **135:** 1071–1083.
51. Faraudo, J., and A. Travesset. 2007. Phosphatidic acid domains in membranes: effect of divalent counterions. *Biophys. J.* **92:** 2806–2818.